Improving the stability of wastewater derived microalgae carbon materials: products characterisation, and kinetic modelling

Ali Akhtar*[1], Ivo Jiříček [2], Vladimir Krepl[1], Abbas Mehrabadi[3], Tatiana Ivanova[1]

1. Department of Sustainable Technologies, Faculty of Tropical AgriSciences, Czech University of Life Sciences Prague, Czech Republic.
2. Department of Power Engineering, University of Chemistry and Technology Prague, Czech Republic.
3. Asset Management Intelligence Support unit, Community Facilities Department, Auckland Council, New Zealand.

*Corresponding author
Ali Akhtar
akhtarczu@gmail.com

Abstract

Microalgae-derived char contains low stability and heating values with relatively high nitrogen content than lignocellulosic char. This study showed that co-pyrolysis helped improve the overall properties of char than individual pyrolysis of these feedstocks. Two batches of experiments were conducted (a) single step pyrolysis and (b) two-step pyrolysis in the range of highest treatment temperature of 400 – 600 °C. Single step pyrolysed char showed, lower aromaticity, higher yield, ash content and heating values of the char than two-step pyrolysed char. Similarly, ignition temperature and activation energy were higher during combustion by single step pyrolysed char than two-step char. Hence, two-step pyrolysed char is suitable in the energy applications, and low-temperature processing (400 – 500 °C) will result in optimum properties in terms of yield and heating values.

Keywords

Biomass; Microalgae; Date palm; Co-pyrolysis; Characterisation

1. Introduction

Organic waste materials are considered as a new energy material in modern research realm and contain the significant value to derive further products for the production of energy in the form of biogas, syngas, biofuels and char [1]. Different kinds of waste are being investigated through pyrolysis from manure [2,3] to agricultural residues [4,5], municipal solid waste [6,7] to industrial waste [8,9]. Although all the waste utilisation techniques are beneficial and provide waste handling option, pyrolysis holds a significant place among all of them. This is due to the versatility of the products obtained through different reaction conditions such as bio-oil and biochar (char). Bio-oil is the result of fast pyrolysis whereas char is the primary product of the slow pyrolysis of lignocellulosic biomass [10]. The peak temperature and types of feedstock also play an essential role in describing the yield and properties of the resultant product.

Char is primarily composed of a carbon-rich material with the loss of weight and volatiles which is formed under the absence of oxygen whereas the feedstock is heated slowly to the peak temperature [1]. Different renewable lignocellulosic feedstock has been reported in several studies. An emerging feedstock which is being considered for char production is microalgae. Microalgae is a unicellular photosynthetic organism which is not visible to the naked eye generally lies in size range of 1-400 µm [11]. Microalgae are a promising feedstock in renewable energy technology which has higher biomass growth than most of the other feedstock and can be used for wastewater treatment [12]. Microalgae use nitrogen and phosphorus during its production hence reducing the concentration of inorganic elements in the wastewater. Microalgae can be used for other purposes in a wastewater treatment facility such as heavy metals removal, or reduction of chemical/biochemical oxygen demand [13] and performs the functions in a relatively short time [14]. While considering the multiple benefits, microalgae are quite a promising feedstock to produce char.

There are different uses of char reported from adsorption of heavy metals as a functional material to combustion in boilers as a coal replacement. Li et al.,[15] have recently reported the effect of miscanthus char on the coal combustion while concluding that char could help in reducing the ignition and burnout temperature if blended with coal at 50%. At another instant, Wang et al.,[16] reported the reduction in PM_1 emissions upon the co-firing of the char and bituminous coal. Han et al., [17] also found a similar observation with torrified char and explained the reason behind the reduction of PM_1 emission is the increment of PM_{1-10} emissions. In another study, char helped in improved combustion and lower burnout temperature at several percentage blends with coal. It was found that char addition with coal $\leq$ 30 % exhibit similar combustion performance equivalent to coal [18].

Different feedstocks have been reported for co-pyrolysis and showed a variety of results. Huang et al., [19] reported the effect of co-pyrolysis of sewage sludge and rice straw/sawdust on the heavy metals leaching in char. Cu, Zn and Ni contents were reduced in the obtained product; however, the surface area and thermal stability decreased with the sawdust biomass. Meng et al., [20] conducted the co-pyrolysis of rice straw with pig manure and recommended to use in 1:3 ratio at 600 °C to reduce the ammonium acetate extractable and Zn and Cu heavy metals in char.

Co-pyrolysis of microalgae and lignocellulosic biomass have also been reported on several occasions for the production of bio-oil. Chen et al., [21] performed a co-pyrolysis of bamboo and microalgae (Nannochloropsis sp.) at 600 °C. It was observed that most of the nitrogen-containing species transferred to the char in the form of pyrrolic-N and quaternary-N and reduced the nitrogen concentration in bio-oil. Duan et al., [22] reported the co-pyrolysis of waste tyre rubber and microalgae in a temperature range (290 – 370 °C) in supercritical ethanol. The microalgae facilitated the conversion of tyre rubber at a lower temperature than the pyrolysis of tyre rubber alone. W. Chen et al., [23] at another instant reported the co-

pyrolysis of lignocellulosic biomass and microalgae. Nitrogen species increased in char (> 75%) and reduced in gas and bio-oil which resulted in nitrogen-doped char yield. Thus, co-pyrolysis of microalgae with other feedstock also showed promising results with the potential to incorporate in biorefineries and produce char of improved properties. Char worked as an adsorbent of nitrogen during the co-pyrolysis of algae with other biomass types during bio-oil production.

Although co-pyrolysis of lignocellulosic biomass and microalgae showed an optimistic trend to improve the properties of bio-oil and gas, further studies are required for exclusive char production. In a recent study by Akhtar et al., [24], microalgae biomass tend to produce less stable char than date palm biomass and have shown the presence of high nitrogen content leading to several types of nitrogen species found on the surface of the char. Congruently, the energy content was also lower as compared to date palm biomass. Due to these recent findings, co-pyrolysis and further two stage pyrolysis was conducted to understand their behaviour in slow pyrolysis technology for char production and its combustion potential. It was assumed that co-pyrolysis will help in coping with these challenges which are currently found by their individually pyrolysed char and two stage pyrolysis will further improve the properties. As both feedstocks are waste-derived materials, hence contain a promising aspect of providing feedstock for biorefineries. Co-pyrolysis of both of this feedstock (date palm branches + wastewater derived microalgae) are conducted, and performance of the resultant product in energy applications concluded.

2. Materials and Methods

2.1 Pyrolysis experiment

Date palm branches (DB) were first dried, cut and crushed into a small particle size of less than 1 mm. Wastewater derived microalgae (WWM) was collected from a wastewater

treatment plant. The individual properties of each of the feedstock can be referred to Akhtar et al., [25] and Akhtar et al., [24]. The derived microalgae contained a number of species including *Actinustrum sp., Coleastrum sp., Diatom sp.,* and *Mucidosphaerium pulchellum*. Co-pyrolysis of the microalgae and date palm biomass was conducted in a fixed bed system. The feedstock was used in a 1:1 ratio and mixed thoroughly before conducting the experiment. The feedstock was put into the sample holder and placed into the reactor before starting the experiment. The initial air in the reactor was vented out by flowing argon gas at 20 cm^3/min. When sufficient flow was detected, the chamber started heating to the highest treatment temperature (HTT) (400 °C, 500 °C and 600 °C) with the residence time of 20 minutes. In single step pyrolysis (CS), the chamber cooled down to normal temperature after reaching HTT and char is recovered, whereas; for two-step pyrolysis (CT), chamber started reheating after the drop of temperature up to 150 °C. For instance, after reaching the HTT of 400 °C with a residence time of 20 minutes at HTT, the temperature drops up to 250 °C and then later started increasing again to HTT (400 °C) with the residence time of 5 minutes. The reactor cooled down after the completion of the second step. This process was also repeated for 500 °C and 600 °C.

2.2 Char characterisation

Char yield was calculated at the end of the experiment through mass change and is presented as a mass yield. BET specific surface area was determined through Coulter SA 3100, working on the principle of N_2 gas phase adsorption at a temperature of 77 K. The samples were degassed at 150 °C under high vacuum for 240 minutes prior to conducting of the experiment. The elemental composition of biomass and char was measured by instrument Elementar Vario EL Cube. To present the variation in values according to co-pyrolysed char, biomass in a 1:1 ratio was mixed and analysed for elemental composition. The energy content of the feedstock and char was determined by Adiabatic Isoperibolic Calorimeter Model

C5000, IKA-Werke, Staufen, Germany. Higher heating values of the char were also calculated based on an elemental composition from the equation (1) given below

$$HHV_T = 0.3491 \times C + 1.1783 \times H + 0.1005 \times S - 0.1034 \times O - 0.015 \times N - 0.0211 \times Ash$$ [26] ……(1)

The combustion and pyrolysis behaviour of the char and the feedstock were examined by the simultaneous TGA-DSC analyser (SDT Q600, TA Instruments, USA). Air and nitrogen atmosphere was employed for combustion and pyrolysis at the flow rate of 100 ml/min and Constant heating rate of 10 K/min. All the samples were processed to granular form passing through the sieve of 125 µm. To analyse the feedstock, both of the biomass samples were mixed in a 1:1 ratio prior to conducting the experiment, to describe the co-combustion and co-pyrolysis conditions for feedstock. The combustion parameters such as ignition temperature, maximum weight loss rate temperature and complete burnout temperature were determined through intersection and conversion method [27].

Surface functional groups were investigated by ATR-FTIR spectroscopy. The spectra were collected at a scan rate of 100 with a spectral resolution of 4 cm^{-1} in the range of 400 cm^{-1} to 4000 cm^{-1}. The atomic elemental composition and nitrogen containing species on the surface of the char products were observed by x-ray photoelectron spectroscopy (XPS) using the instrument ESCA Probe P.

3. Results and discussion

3.1 Char characteristics

Yield, surface area and heating values of the char are presented in *Table 1*. Yield is decreasing while the surface area is increasing with the increase of temperature. The yield and surface area range was observed to be between 30 – 40% and 1 – 2 m^2/g respectively for all the samples. CT showed a minor decrease in surface area as well as a decrease in yield

than CS. At higher temperatures, yield difference reduces to less than 1%. Overall, more than 8% decrease in yield observed for HTT 600 °C than 400 °C. Likewise, heating values also decreased with an increase in temperature. Conversely, the ash content increases with the increase in HTT from 21 to 27% in CS samples and 20 to 26% in CT samples.

Table 1 Yield, surface area, ash and energy values of the char (CS = Single step, CT = Two step, & 4, 5 and 6 represents 400, 500 and 600 °C respectively)

Samples	**Mass yield (%)**	**Surface Area (m^2/g)**	**Ash content (%)**	**HHV_M (MJ/kg)**	**HHV_T (MJ/kg)**
CS-4	40.03	1.013	21.3	24.47	23.36
CS-5	33.51	1.471	24.4	23.62	21.75
CS-6	31.02	2.022	27.4	23.59	22.14
CT-4	38.40	1.055	20.1	23.20	22.54
CT-5	32.17	1.335	26.2	22.46	22.34
CT-6	30.29	1.967	26	22.82	23.22

HHV_T Theoretical higher heating value
HHV_M Measured higher heating value

Ultimate analysis of the feedstock and all the char samples was conducted to determine the C, H, N, S and O contents with H/C, O/C and (O+N)/C atomic ratios (Supplementary material). Increasing the treatment temperature increased the carbon content and decreased the hydrogen and nitrogen content in the char. On the contrary, both feedstocks (DB+WWM) in the combined form showed a higher amount of hydrogen and nitrogen and lower carbon content than the chars. This also agrees with other studies which reported the relatively high nitrogen content of microalgae [21,28]. Co-pyrolysis reduced the overall nitrogen concentration in char and CT slightly reduced the nitrogen and hydrogen content than CS.

3.2 Atomic ratios and Van Krevelen diagram

The atomic ratios (H/C and O/C) of the feedstock and chars are presented in the Van Krevelen diagram (*Figure 1*) showing the decrease in ratios as the temperature increases. Feedstock tends to show higher H/C and O/C ratios than their respective chars [29]. Lower O/C ratios represent the formation of graphite-like structures through a structural arrangement of aromatic rings [30]. The lower ratios in char depict a reduction in volatile matter content and increase in aromaticity [31]. The H/C ratios were significantly lower than most of the chars reported [31–33] indicating a significant increase in aromaticity. Both treatment processes showed a decrease in ratios with the increase in temperature.

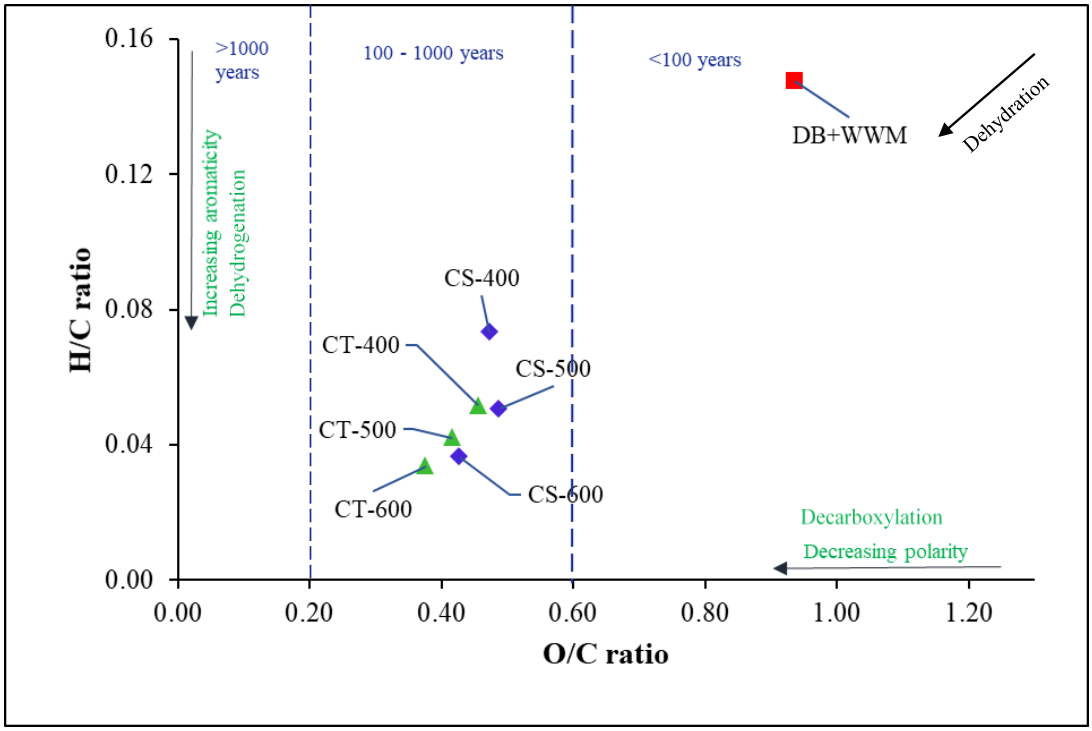

Figure 1 Van Krevelen diagram of O/C and H/C atomic ratios. The dotted line at 0.6 and 0.2 O/C ratio separating the range of half-life of char produced [45]

However, CT revealed a rather significant decrease in which CT at 500 °C showed equivalent ratios to the CS at 600 °C. It is worthwhile to note that O/C ratios reduced comparatively at 600 °C for CS samples than 400 °C and 500 °C. Chiodo et al., [34] previously reported that algae char tend to show high O/C ratios than lignocellulosic biomass derived char when pyrolysed individually at all HTTs (400, 500 and 600 °C). This phenomenon also observed in a recent study by Akhtar et al., [24] for wastewater derived microalgae. Hence, a co-pyrolysis is a suitable approach to gain overall lower O/C ratio in the end product, and CT can further reduce the atomic ratio to increase the aromaticity of the char.

The regression analysis was performed to determine the influence of the H/C, N/C and mass yield on the ash production in a co-pyrolysed char (*Figure 2*). All three parameters showed moderate to the high coefficient of determination with substantially low p-values. However, the trend shows a negative slope such as increasing atomic ratios and yield decreased the ash content of char.

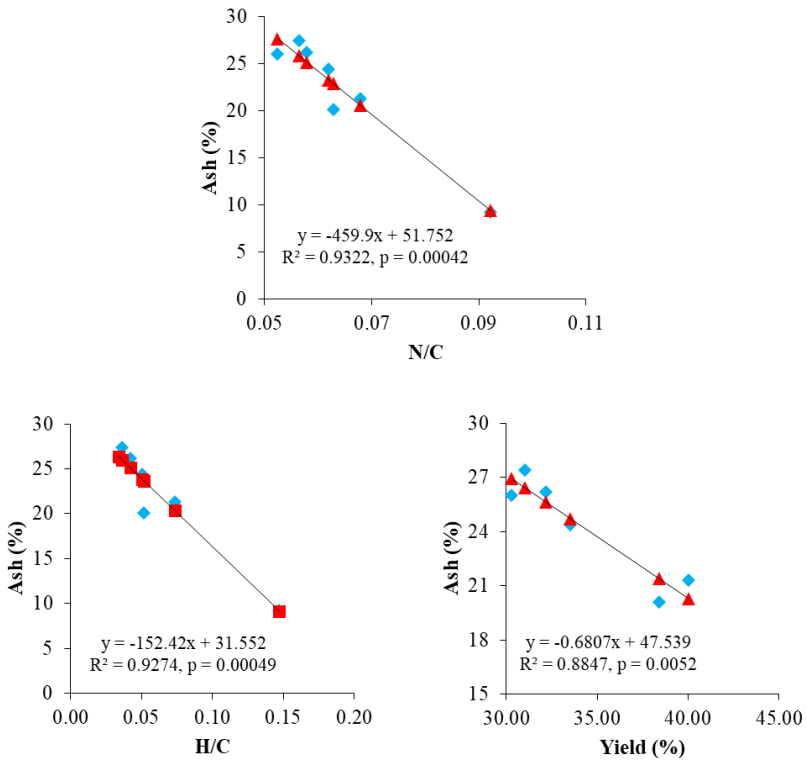

Figure 2 Ash correlation with N/C, H/C and yield with the coefficient of determination and p values.

3.3 Fourier Transform Infrared Spectroscopy

The presence of functional groups in the char and feedstock was analysed by ATR-FTIR spectroscopy. The changes in the patterns of functional groups due to thermal treatment are quite visible among samples. The spectra of feedstock and char can be seen in Supplementary material. Different treatment temperatures showed peaks of different intensities. The samples subjected to the two-step approach also showed significant changes at 500 °C and 600 °C, however, the spectra seems to be similar at 400 °C HTT with similar intensities. WWM feedstock showed peaks at 996 cm^{-1}, 1375 cm^{-1}, 1452 cm^{-1}, 1625 cm^{-1}, 2917 cm^{-1}, 3328 cm^{-1} corresponding to the =C – H bending vibration [35], CH_3 C – H bending vibration [36], C = C stretching [37], N – H bending [38], C – H stretching [37,39], O – H stretching vibration. DB feedstock, on the other hand, contained relatively higher peaks at 1031 cm^{-1} and 3328 cm^{-1}.

DB feedstock showed peaks at 1031 cm^{-1}, 1240 cm^{-1}, 1367 cm^{-1}, 1507 cm^{-1} representing C-O stretching [37], O=C – O – C stretching [37], $CH(CH_3)_2$ bending and N – H bending vibration [38] respectively while the rest of the peaks were similar to WWM feedstock. Char clearly showed a different pattern than the feedstock resulting in the appearance of some peaks while few peaks completely disappeared. For instance, peaks around 860 cm^{-1} and 870 cm^{-1} for =C – H bending vibration [40] did not appear in the char with HTT of 400 °C.

However, peaks were started forming at 500 °C and becomes sharp at 600 °C. This represents the aromatic C – H out of plane deformation which indicates the condensation into larger sheets from small units [41]. Similarly, relatively small peaks appeared at 1370 cm^{-1} for CH_3 C-H bending vibration [39] at 400 °C and 500 °C whereas disappeared at 600 °C. The peaks around 1100 cm^{-1} representing C – O stretch [39,40] become significantly broad at 600 °C, however, appeared as a minor peak at 400 °C. The N – H bending vibration at 1557 cm^{-1} were also of higher intensity at 400 and 500 °C rather than 600 °C. The spectra of char

showed an upward shift of baseline with the increase in HTT which is due to condensed aromatic structures containing low-energy electron excitation [41].

The peaks at 2910 cm^{-1} and 3325 – 3355 cm^{-1} corresponding to C – H stretching [37] and Alcohol O-H broad stretching vibration [37] respectively, did not appear at 600 °C which was the most significant peak in DB. C – H stretching in chars at 400 °C shows the carbonisation step is incomplete [42]. The difference between CS and CT peaks are quite significant at 600 °C and reduces as the HTT decreases. It can be seen that peaks at 400 °C are of quite similar intensity for CS and CT with a marginal difference around 1200 cm^{-1} and 1580 cm^{-1}. Peak shift was not significant in any of the samples, however, peaks were of higher intensity at 500 °C for CT than CS and at 600 °C vice versa. Although CS and CT showed nearly similar peaks, however, the operating temperature of 500 °C seems to contain the middle ground where the functional groups are present, not available at 400 and 600 °C.

3.4 X-ray Photoelectron Spectroscopy

The data on the atomic elemental composition of the char samples were observed through XPS technology for C1s, O1s, N1s, Ca2p, Cl2p and K2p. Other elements such as Na1s, Si2s, S2s and P2p of minor percentages were also observed in a few samples. These elements were mostly found in samples subjected to a high treatment temperature and in two-step pyrolysis. The atomic percentage of carbon is relatively higher at lower HTT whereas it is decreasing with the increasing temperature. Upon subjecting to the two-step pyrolysis (CT), the variation in carbon content was not significant. All the samples showed the atomic ratio of 74 – 77% of carbon on the surface. Oxygen concentration, on the other hand, was found to be highest at 500 °C in both CS and CT treatment processes. Oxygen was found to be increased in CT samples than CS, indicating the presence of higher oxygen functional groups. Conversely, N

was found to be lowest in CT samples and Ca showed the maximum concentration at 600 °C for both treatment processes.

Nitrogen species investigated in char samples subjected to CS and CT. It is important to note that these values depict the char surface properties rather than the bulk presence of the nitrogen in the samples. Pyridinic, quaternary and pyrrolic nitrogen species were the highest among all of them in CT samples and, pyridinic and pyrrolic in CS samples except CS-4 which also showed the presence of quaternary-N (Supplementary materials). Furthermore, pyridinic – N and pyrrolic – N substantially increased with the decrease of oxidized – N and quaternary – N upon increasing the HTT. Oxidized and quaternary – N was removed altogether when HTT approached 500 °C in CS. However, amine – N concentration seems to be highest at HTT 500 °C. A contrast behaviour in nitrogen species was observed in CT samples, showing quaternary-N was available in all of the samples. Oxidized – N showed similar behaviour and reduced to less than 1% after 500 °C HTT. This can be seen that overall nitrogen concentration decreased with the increase in HTT and the further decrease was observed in CT samples, causing most of the nitrogen to convert to the gaseous phase. The left out nitrogen was present in the form of pyridinic, pyrrolic, and amine nitrogen species which were also the dominant nitrogen species in a study presented by W. Chen et al., [23] at 600 °C. Nitrogen-doped char holds the potential to use in different applications such as reducing the NO_x reduction when co-combusted with coal [43] and superior electrochemical efficiency with potential supercapacitors applications [44].

3.5 TGA-DSC analysis

3.5.1 Char Combustion

A simultaneous thermogravimetric – differential scanning calorimetric analysis of the biomass and char samples was conducted to determine the weight loss and degradation

pattern during combustion and pyrolysis. Co-combustion of feedstock (date palm branches and microalgae) showed a slightly different behaviour than the combustion of co-pyrolysed char (*Figure 3*). The moisture contained in the feedstock was more than 6 %, whereas, for the chars, it was in the range of 4 – 5 % of its total weight. Degradation stages noted in DTG curves verified 2 stage devolatilization in which feedstock showed the first peak around 300 °C and a second peak around 490 °C. All the chars, on the other hand, showed the first peak after 400 °C, exhibiting higher stability than the feedstock. The degradation rate at first peak gradually increased with the increase of HTT (400 > 500 > 600). CS relatively showed lower peak than CT at 400 and 600 °C.

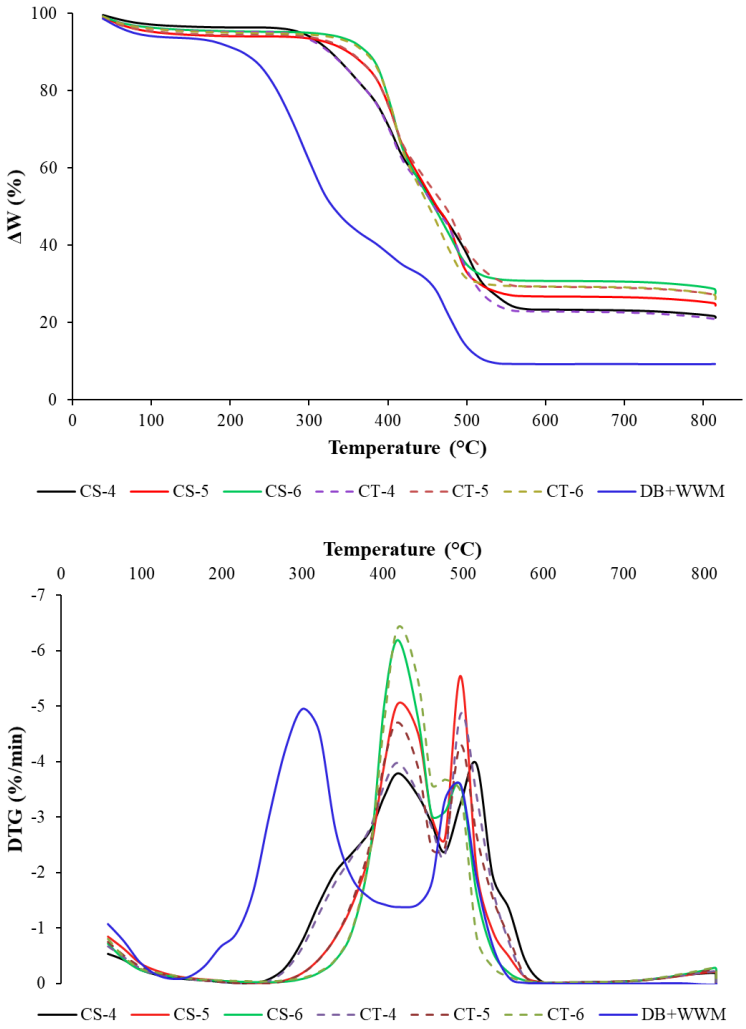

Figure 3 TGA and DTG curves of biomass and chars produced at 400, 500 and 600 °C in air atmosphere

The second peak for the CT-6 sample seems to disappear, however, a small second peak can be seen in the CS sample (CS-6). CT has also shown contrast behaviour than CS in other samples, CS-4 exhibit reduced second peak and CS-5 the highest peak, whereas, CT-5 showed the lowest second peak. The change in degradation pattern is due to lower fixed carbon content upon reaching the second stage. This might be the reason for disappearing the second peak in CT-6 samples and contributing towards higher first peak than the rest of the samples. Thus, CT-6 might have the potential to fully utilise the char at a lower temperature than its peers. The range for overall combustion of feedstock is 241 – 557 °C, whereas, this range reduced for CT samples (340 – 577 °C). DSC curves have shown a comparatively similar trend to DTG for heat flow, however, the change is distinctive for CS-4 and CT-4 samples, showing three peaks with gradually increasing intensity (Supplementary materials). The first peak reduced its intensity in CT-4 samples than CS-4. Unlike, DTG, feedstock exhibit second highest peak, showing the contributing potential of energy in the second phase despite low degradation.

Combustion parameters have been calculated to view the overall combustion behaviour from starting the ignition towards complete burnout of the samples. It was shown that the char has long burning time and contain the ability to generate energy for the long duration of time than co-combustion of feedstock (*Table 2*). This is evident from the measured heating values as well. CT relatively reduced the ignition temperature of chars than CS chars. Although, conversion method shows 95% and 88% burnout of the feedstock samples, however, this might not generate a significant amount of energy after second stage degradation majorly after 600 °C. The change in weight loss is less than 1% for biomass and less than 5% for all char samples from 600 to 800 °C. The economic feasibility of char concerning its remaining energy potential after second stage degradation could be explored in future studies and generalise the char and biomass for its energy generation potential. Statistical analysis was

also performed between ignition temperature and burnout temperature to determine the significance and correlation coefficient. Burnout temperature have shown a high correlation coefficient (R^2 = 0.96) in relation to ignition temperature with p-value 6.5E-05 < 0.5 (Supplementary materials).

Table 2 Co-combustion of date palm biomass and wastewater derived microalgae and their co-pyrolysed char

Samples	T_i (°C)	T_{max} (°C)	T_b (°C)	DTG_{max}	E (kJ/mol)	R^2
DB+WWM	241	301	536	-4.95	160.5	0.93
CS-4	343	514	757	-3.96	150.3	0.90
CS-5	362	497	777	-5.55	128.3	0.90
CS-6	367	419	797	-6.19	134.3	0.91
CT-4	339	499	777	-4.87	133.7	0.92
CT-5	351	419	777	-4.71	123.3	0.93
CT-6	353	420	797	-6.42	132	0.90

T_i, T_{max}, T_b, DTG_{max}, and E represents the ignition temperature, maximum weight loss rate temperature, burnout temperature, maximum weight loss rate and activation energy respectively.

3.5.2 Kinetic modelling

The activation energy of the samples can be calculated through the Arrhenius kinetic model, and it can be determined through the following equations (7-10)

$$k(T) = Ae^{(-\frac{E}{RT})} \quad \text{..... (7)}$$

$$\frac{d\alpha}{dt} = Ae^{(-\frac{E}{RT})}(1-\alpha)^n \quad \text{.....(8)}$$

$$\alpha = \frac{\omega_\varphi - \omega}{\omega_\varphi - \omega_f} \quad \text{.....(9)}$$

E is the activation energy ($kJmol^{-1}$), R is the gas constant (8.34 $Jk^{-1}mol^{-1}$), T is the absolute temperature (K), and A is the pre-exponential factor (s^{-1}), n is the order of reaction, and α is the conversion rate.

After rearranging and integration method (Coats – Redfern method) applied, the equation changed into the following form

$$\ln[-\frac{\ln(1-\alpha)}{T^2}] = \ln\frac{AR}{\beta E} - \frac{E}{RT} \quad \text{.....(10)}$$

β is the heating rate (°$Cmin^{-1}$ or $Kmin^{-1}$)

The kinetic illustration is presented in *Figure 4***,** and activation energy (E) is calculated from the slope of the curves for the overall combustion process and is presented in *Table 2*. The lower the activation energy, the lower the energy required to begin the combustion process. It can be seen that all of the chars have shown overall lower activation energy according to the co-combustion of the feedstock. The lowest amount of activation energy was noted by CT chars, and at 500 °C HTT char have shown relatively less activation energy both for CS and CT than the rest of the samples. CS samples showed the range of activation energy from 128 kJ/mol to 150 kJ/mol which is dropped in case of CT and found in the range of 123 to 133 kJ/mol. CS-5 and CT-5 both samples reduced the activation energy more than 30 kJ/mol according to the feedstock. Regression analysis showed a high coefficient of correlation in all of the samples, exhibiting $R^2 \geq 0.90$.

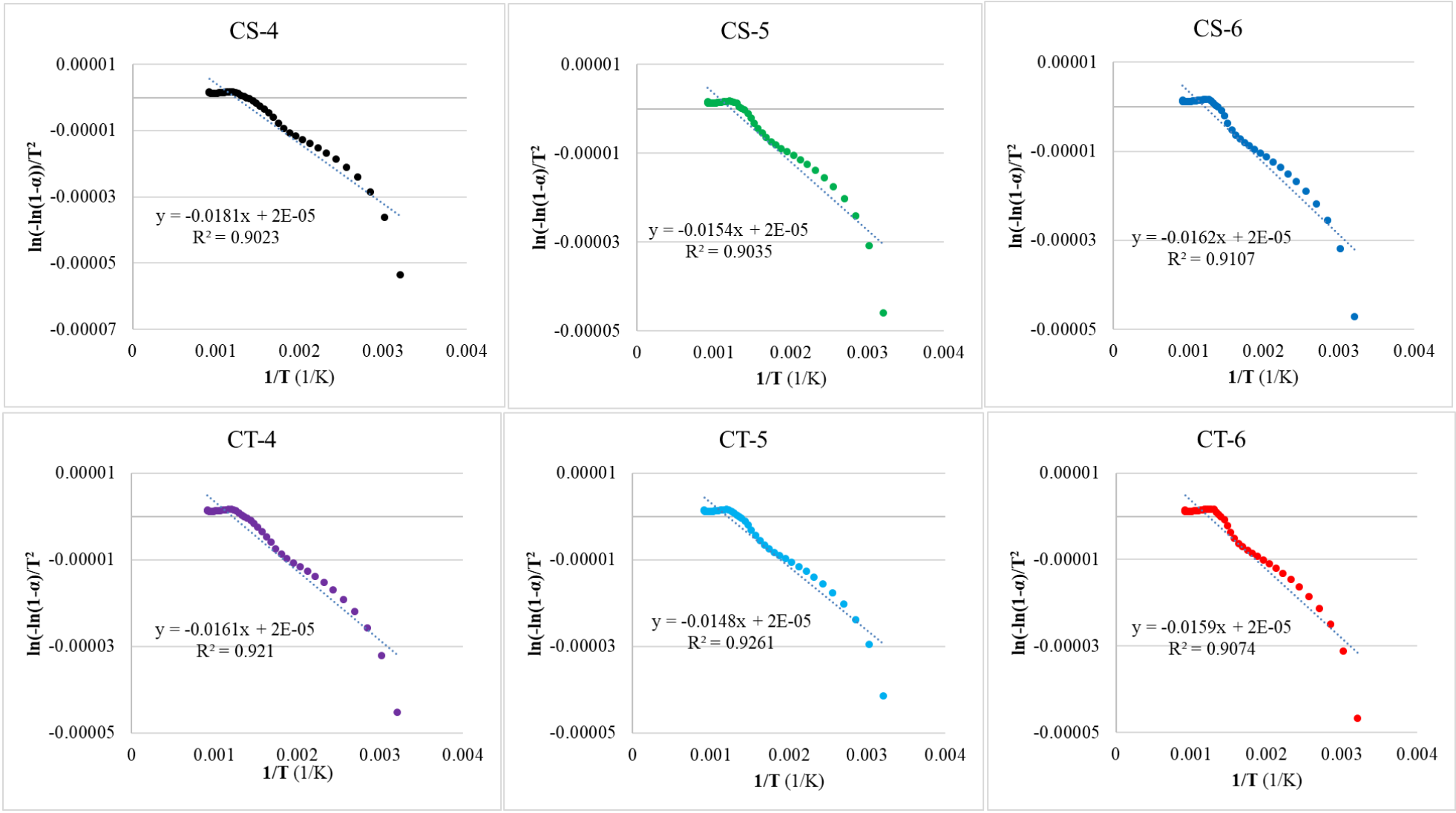

Figure 4 Kinetic illustrations of chars subjected to combustion

3.5.3 Char Pyrolysis

A similar set of experiments conducted in a nitrogen environment to illustrate the pyrolysis conditions for the concerned samples (*Figure 5*). It can be seen that char has shown single stage degradation with a couple of minor peaks after 800 °C as compared to two-stage combustion. Degradation can be seen as limited with maximum weight loss occurred in samples subjected to 400 °C HTT. The increase in temperature resulted in less degradation with high char content. Although degradation happened in small percentage than combustion, however, it continuous to devolatilize for a longer duration. There is a small degradation noted between 800 – 1000 °C which resulted in a weight loss of more than 10% in this range in all of the samples of CS and CT. CT samples reduced the weight loss further around 3-4 % at 400 and 600 °C HTT.

Weight loss rate curve showed a comprehensive outlook of the samples in which the highest peak shifted for CS-5, CS-6, CT-5 and CT-6 samples from 400 – 500 °C towards 500 – 600 °C. Weight loss rate reduced substantially after 500 °C with a sudden decline in a peak in CS-4 and CT-4 samples, whereas, it continues to increase for the rest of the samples. This might be due to the higher char's stability treated at high temperatures as shown in Van Krevelen diagram (*Figure 1*). Combined feedstock also showed single stage degradation, hence, confirming the single step pyrolysis of the biomass. The smooth curve could be observed after 600 °C, however, weight loss continues to occur up to 10% of the total weight from 600 °C to 1000 °C. The regression analysis of mass yield and energy yield showed a high coefficient of determination ($R^2 = 0.969$) and p-value (0.00035) substantially lower than 0.05 (Supplementary material). The higher mass yield translates to higher energy yield.

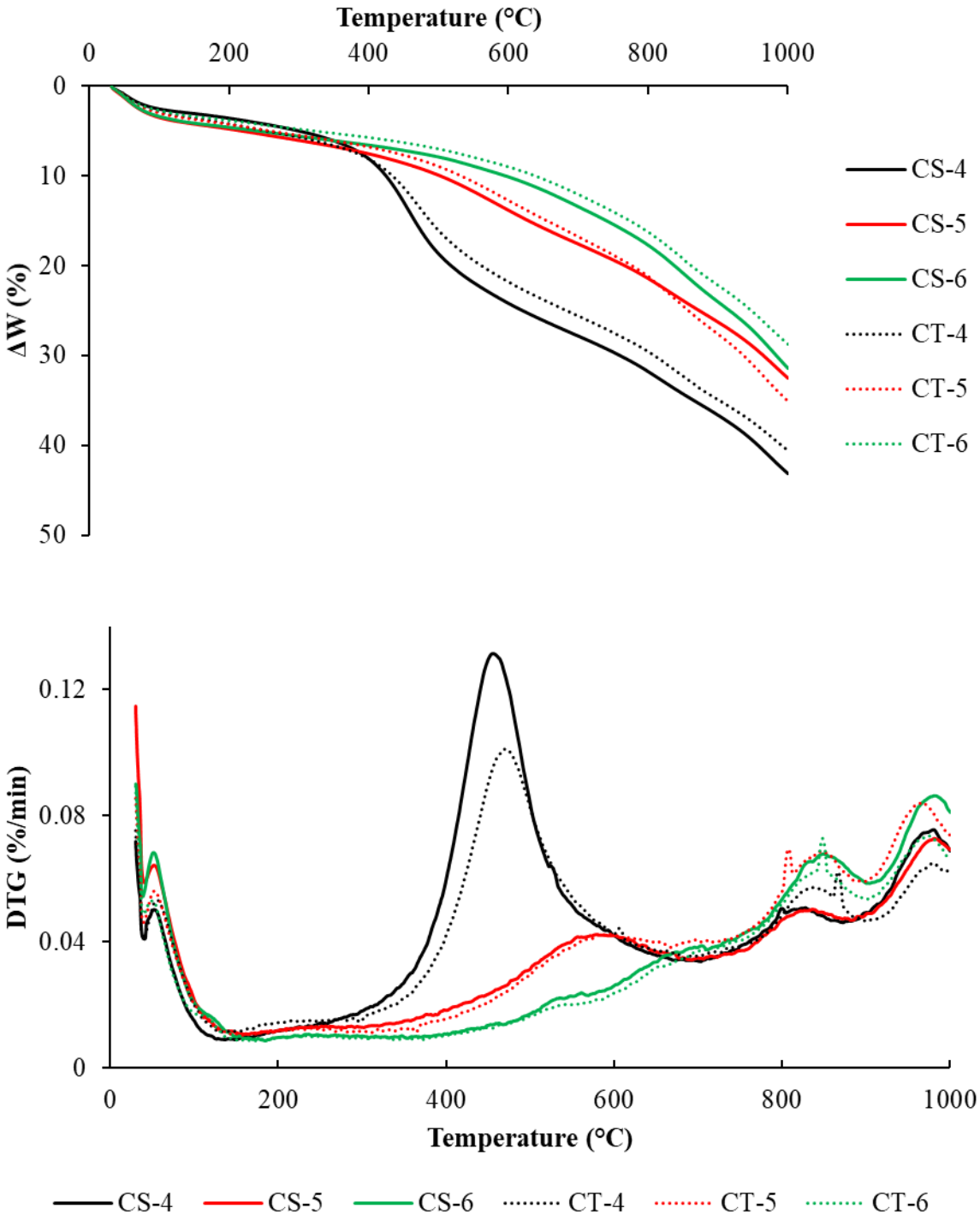

Figure 5Thermal analysis of co-pyrolysed char in nitrogen atmosphere

4. Conclusion

Co-pyrolysis of date palm branches and wastewater derived microalgae was conducted at 400, 500 and 600 °C for a single step and two step pyrolysis. Char aromaticity increased, and mass yield decreased substantially with the increase in treatment temperature in both CS and CT from 40% to 30% by weight. Nitrogen concentration was decreased with the increase in temperature, and similar results were found for nitrogen species on the surface of the char. The nitrogen-doped char holds the potential to be used in a range of applications from the reduction of NO_x emissions to supercapacitors.

Combustion of the feedstock and the char samples produced at 400 and 500 °C showed two-stage degradation whereas pyrolysis showed single stage degradation. 500 °C is the optimum treatment temperature for two-step pyrolysis to gain the lowest activation energy during combustion, moderate heating values. Similarly, the activation energy of the subsequent pyrolysis of char samples also decreased than their feedstock. CT samples at treatment temperatures (≥ 500 °C) showed higher activation energy than CS samples. It can be concluded that co-pyrolysed char from CT samples contain the higher combustion properties and can be used with coal for partial fuel substitution in combustion chambers.

5. References

1 A. Akhtar, V. Krepl and T. Ivanova, *Energy & Fuels*, 2018, **32**, 7294–7318.

2 N. Scarlat, F. Fahl, J. F. Dallemand, F. Monforti and V. Motola, *Renew. Sustain. Energy Rev.*, 2018, **94**, 915–930.

3 F. Tasnim, S. A. Iqbal and A. R. Chowdhury, *Renew. Energy*, 2017, **109**, 434–439.

4 S. Kamel, H. A. El-Sattar, D. Vera and F. Jurado, *Renew. Sustain. Energy Rev.*, 2018, **94**, 28–37.

5 F. Valenti, S. M. C. Porto, R. Selvaggi and B. Pecorino, *J. Environ. Manage.*, 2018, **223**, 834–840.

6 C. Gopu, L. Gao, M. Volpe, L. Fiori and J. L. Goldfarb, *J. Anal. Appl. Pyrolysis*, 2018, **133**, 48–58.

7 A. T. Sipra, N. Gao and H. Sarwar, *Fuel Process. Technol.*, 2018, **175**, 131–147.

8 A. Fernandez, A. Saffe, R. Pereyra, G. Mazza and R. Rodriguez, *Appl. Therm. Eng.*, 2016, **106**, 1157–1164.

9 R. Kumar Singh, B. Ruj, A. Jana, S. Mondal, B. Jana, A. Kumar Sadhukhan and P. Gupta, *J. Anal. Appl. Pyrolysis*, , DOI:10.1016/j.jaap.2018.08.011.

10 D. Mohan, A. Sarswat, Y. S. Ok and C. U. Pittman, *Bioresour. Technol.*, 2014, **160**, 191–202.

11 K. L. Yu, P. L. Show, H. C. Ong, T. C. Ling, J. Chi-Wei Lan, W. H. Chen and J. S. Chang, *Energy Convers. Manag.*, 2017, **150**, 1–13.

12 N. Abdel-Raouf, A. A. Al-Homaidan and I. B. M. Ibraheem, *Saudi J. Biol. Sci.*, 2012, **19**, 257–275.

13 H. J. Choi and S. M. Lee, *Environ. Eng. Res.*, 2012, **17**, 3–8.

14 A. Mehrabadi, R. Craggs and M. M. Farid, *Bioresour. Technol.*, 2015, **184**, 202–214.

15 Y. H. Li, H. T. Lin, K. L. Xiao and J. Lasek, *Energy*, 2018, **163**, 180–190.

16 W. Wang, C. Wen, C. Li, M. Wang, X. Li, Y. Zhou and X. Gong, *Fuel*, 2019, **240**, 278–288.

17 J. Han, D. Yu, X. Yu, F. Liu, J. Wu, X. Zeng, G. Yu and M. Xu, *Proc. Combust. Inst.*, 2019, **37**, 2733–2740.

18 J. Mundike, F. X. Collard and J. F. Görgens, *Fuel*, 2018, **225**, 62–70.

19 H. jun Huang, T. Yang, F. ying Lai and G. qiang Wu, *J. Anal. Appl. Pyrolysis*, 2017, **125**, 61–68.

20 J. Meng, S. Liang, M. Tao, X. Liu, P. C. Brookes and J. Xu, *Chemosphere*, 2018, **200**, 344–350.

21 W. Chen, Y. Chen, H. Yang, M. Xia, K. Li, X. Chen and H. Chen, *Bioresour. Technol.*, 2017, **245**, 860–868.

22 P. Duan, B. Jin, Y. Xu and F. Wang, *Chem. Eng. J.*, 2015, **269**, 262–271.

23 W. Chen, H. Yang, Y. Chen, K. Li, M. Xia and H. Chen, *Environ. Sci. Technol.*, 2018, **52**, 9514–9521.

24 A. Akhtar, I. Jiříček, T. Ivanova, A. Mehrabadi and V. Krepl, *Int. J. Energy Res.*, 2019, **43**, 4403–4416.

25 A. Akhtar, T. Ivanova, I. Jiříček and V. Krepl, *J. Renew. Sustain. Energy*, 2019, **11**, 13102.

26 S. A. Channiwala and P. P. Parikh, *Fuel*, 2002, **81**, 1051–1063.

27 J. J. Lu and W. H. Chen, *Appl. Energy*, 2015, **160**, 49–57.

28 W. Chen, K. Li, M. Xia, H. Yang, Y. Chen, X. Chen, Q. Che and H. Chen, *Energy*, 2018, **157**, 472–482.

29 L. Leng, H. Huang, H. Li, J. Li and W. Zhou, *Sci. Total Environ.*, 2019, **647**, 210–222.

30 K. Jindo, H. Mizumoto, Y. Sawada, M. A. Sanchez-Monedero and T. Sonoki, *Biogeosciences*, 2014, **11**, 6613–6621.

31 K. H. Kim, J. Y. Kim, T. S. Cho and J. W. Choi, *Bioresour. Technol.*, 2012, **118**, 158–162.

32 M. Uchimiya, L. H. Wartelle, K. T. Klasson, C. A. Fortier and I. M. Lima, *J. Agric. Food Chem.*, 2011, **59**, 2501–2510.

33 Y. Lee, P. R. B. Eum, C. Ryu, Y. K. Park, J. H. Jung and S. Hyun, *Bioresour. Technol.*, 2013, **130**, 345–350.

34 V. Chiodo, G. Zafarana, S. Maisano, S. Freni and F. Urbani, *Fuel*, 2016, **164**, 220–227.

35 M. Jouiad, N. Al-Nofeli, N. Khalifa, F. Benyettou and L. F. Yousef, *J. Anal. Appl. Pyrolysis*, 2015, **111**, 183–190.

36 L. J. Leng, X. Z. Yuan, H. J. Huang, H. Wang, Z. Bin Wu, L. H. Fu, X. Peng, X. H. Chen and G. M. Zeng, *Fuel Process. Technol.*, 2015, **129**, 8–14.

37 P. Rousset, C. Aguiar, N. Labbé and J. M. Commandré, *Bioresour. Technol.*, 2011, **102**, 8225–8231.

38 M. M. Phukan, R. S. Chutia, B. K. Konwar and R. Kataki, *Appl. Energy*, 2011, **88**, 3307–3312.

39 S. W. Park, C. H. Jang, K. R. Baek and J. K. Yang, *Energy*, 2012, **45**, 676–685.

40 P. Huang, C. Ge, D. Feng, H. Yu, J. Luo, J. Li, P. J. Strong, A. K. Sarmah, N. S. Bolan and H. Wang, *Sci. Total Environ.*, 2018, **616**–**617**, 1384–1391.

41 M. Keiluweit, P. S. Nico, M. G. Johnson and M. Kleber, *Environ. Sci. Technol.*, 2010, **44**, 1247–1253.

42 C. H. Chia, B. Gong, S. D. Joseph, C. E. Marjo, P. Munroe and A. M. Rich, *Vib. Spectrosc.*, 2012, **62**, 248–257.

43 X. Wang, J. Gao, Z. Sun, J. Cheng, L. Xu, Q. Du and Y. Qin, *Can. J. Chem. Eng.*, 2018, **96**, 873–880.

44 M. Demir, S. K. Saraswat and R. B. Gupta, *RSC Adv.*, 2017, **7**, 42430–42442.

45 K. A. Spokas, *Carbon Manag.*, 2010, **1**, 289–303.